

Analysis of impact toughness and the critical stress intensity factor K_{Ic} in ferrite-austenite welded joints with different heat input

Aleksandar G. Bukvić^a, Dalibor P. Petrović^b,
Igor Z. Radisavljević^c, Saša S. Dimitrić^d

^a University of Defense in Belgrade, Military Academy,
Belgrade, Republic of Serbia,
e-mail: a_bukvic@yahoo.com, **corresponding author**,
ORCID iD:  <https://orcid.org/0000-0002-3025-8446>

^b University of Defense in Belgrade, Military Academy,
Belgrade, Republic of Serbia,
e-mail: dalibor.petrovic140@gmail.com,
ORCID iD:  <https://orcid.org/0000-0001-6092-5695>

^c Ministry of Defense of the Republic of Serbia,
Military Technical Institute, Belgrade, Republic of Serbia,
e-mail: radisavljevicigorbg@gmail.com,
ORCID iD:  <https://orcid.org/0000-0002-8523-0993>

^d University of Defense in Belgrade, Military Academy,
Belgrade, Republic of Serbia,
e-mail: sasa.dimitric@mod.gov.rs,
ORCID iD:  <https://orcid.org/0000-0003-3547-7047>

DOI: 10.5937/vojtehg71-42358; <https://doi.org/10.5937/vojtehg71-42358>

FIELD: mechanical engineering, mechanical materials, fracture mechanics
ARTICLE TYPE: original scientific paper

Abstract:

Introduction/purpose: Constructions always have several critical points that can be sources of possible defects. All these critical places must be taken into account in safety assessment where the most unfavorable exploitation factors are considered and the local safety of a joint is assessed. Today, joints of various compositions are becoming more frequent in metal constructions. Due to the requirements of economy and ecology, welded joints of microalloyed ferritic steels with high-alloyed austenitic steels are increasingly encountered during the construction of power plants, chemical facilities, etc. Tests of such welded joints have been performed on tanks for oil derivatives, where parts of the tank shell are made of microalloyed ferritic steel and the roof structure is made of high-alloyed austenitic steel.

Methods: In the paper, an experimental analysis of crack propagation in an austenitic-ferritic welded joint was performed. The welding was performed by the MIG welding process with two different heat inputs, and the same filler material MIG 18/8/6 was used. Two types of welded plates were tested.

the characteristics of the base, filler and auxiliary materials and welding technologies are given. Notched test specimens with an initiated crack-type fracture were made in order to determine the impact properties and fracture mechanics parameters.

The results: The research carried out within this study aimed to compare the obtained results of the impact toughness and fracture toughness at flat deformation in a ferrite-austenitic welded joint. An evaluation of the results obtained during the testing of the experimental plates welded with different amounts of heat input is also given.

Conclusion: These test results established the dependence of the geometry of a propagating crack and the stress conditions for further crack propagation. It is possible to determine the values of the parameters that describe the behavior of the material, both in linear-elastic and in elasto-plastic fracture mechanics.

Key words: ferrite-austenitic welded joint, impact toughness, critical stress intensity factor K_{Ic} .

Introduction

Impact toughness tests are important when considering a material's tendency to brittle fracture. Impact tests are performed in order to determine total energy (impact toughness) as well as energy of crack creation and growth in critical parts of welded joints (Rabbolini et al, 2015; Bukvić, 2012).

Efforts are constantly made to study the causes of material fatigue and to mitigate its consequences. Material failure caused by fatigue is the most common form of failure in practice. Such fractures occur at stress values that are lower than the tensile strength even in low-strength plastic materials (Bukvić, 2012; Rabbolini et al, 2015). A large number of structure fractures which occur during exploitation at lower than permissible stress levels indicate the risk of brittle fracture (Bukvić, 2012; Rabbolini et al, 2015).

When studying fatigue of materials using fracture mechanics, it is assumed that there is an initial crack or that the period of its formation is short or negligible. Determining the working life of a structure is reduced to predicting the time of crack growth. The process of material fatigue under variable loading can be divided into three phases (Zerbst et al, 2015), as in Figure 1:

1. *crack formation* (threshold value below which a fatigue crack has no conditions for growth);

2. crack propagation up to a critical value (area of application of the Paris equation); and
3. unstable fracture of the final part of the section (ΔK_c at which a fracture occurs).

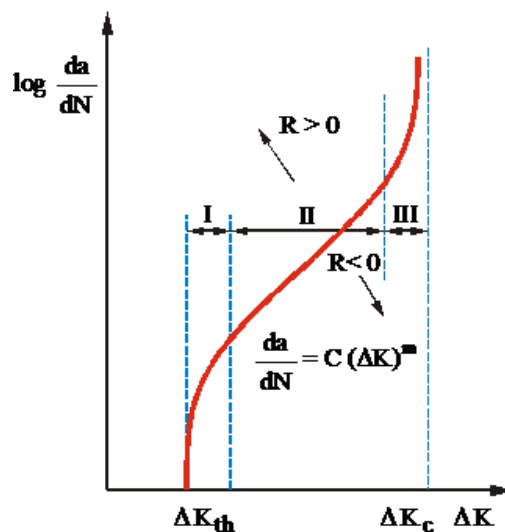


Figure 1 – Typical appearance of the fatigue crack growth curve as a function of ΔK
 Рис. 1 – Типичный вид кривой роста усталостной трещины в функции от ΔK
 Слика 1 – Типичан изглед криве раста заморне прслине у функцији од ΔK

Fatigue occurs as a result of plastic deformation during the stages of crack formation and growth. Until the final failure of the material, fatigue spreads in the form of plastic failure of the material, although this plasticity, of a completely local nature, is limited only to the process zone. The fatigue effect is a cumulative action of microscopically limited events which can add up to several million in a single fatigue process. Therefore, it is difficult to predict in advance the service life of a structural element that has begun to break and is permanently loaded with a variable load (Zerbst et al, 2015).

The fracture toughness test at flat deformation K_{Ic} was carried out in order to determine the critical factor of stress intensity, K_{Ic} , i.e. the evaluation of the behavior of the components of a welded joint, weld metal and the HAZ in the presence of a crack-type defect as the most dangerous of all defects in structural materials, especially welded joints (Bukvić, 2012; Zerbst et al, 2015).

Chemical and mechanical characteristics of materials and welding technology

Base materials

Two base materials were used for welding: microalloyed steel S500NL1, under the commercial name NIOMOL 490K with a thickness of 16 mm (marked with M) and high-alloyed steel X6CrNiMoTi 17 12 2 according to EN 10088 (Č.4574 according to SRPS EN 10088-1) with a thickness of 12 mm (marked with V) (Bukvić, 2012). Table 1 shows the chemical compositions and Table 2 shows the mechanical properties of the base materials.

Table 1 – Chemical compositions of the base materials (Bukvić, 2012)
Таблица 1 – Химический состав основных материалов (Bukvić, 2012)
Табела 1 – Хемијски састав основних материјала (Bukvić, 2012)

	C	Si	Mn	P	S	Cr	Ni	Cu	Al	Mo	Ti	V	Nb
M	0.10	0.38	0.64	0.014	0.02	0.76	0.10	–	–	0.33	–	0.02	–
V	0.04	0.35	1.73	0.031	0.004	17.9	11.6	0.18	0.061	2.16	0.38	0.079	0.016

Table 2 – Mechanical properties of the base materials (Bukvić, 2012)
Таблица 2 – Механические свойства основных материалов (Bukvić, 2012)
Табела 2 – Механичке особине основних материјала (Bukvić, 2012)

Base materials	Yield stress $R_{0.2}$ [MPa]	Tensile strength R_m [MPa]	Elongation A [%]	Contraction Z [%]
M	497	584	20	65
V	321	596	37	53

Filler material

Welding was performed using filler material MIG 18/8/6, produced in Železarne ACRONI, Jesenice, Slovenia (Bukvić, 2022; Jesenice Ironworks, 2005). Table 3 shows the chemical compositions and Table 4 shows the mechanical properties of the welding wire.

The filler material MIG 18/8/6 was selected based on recommendations from the literature (Jovicic, 2007; Bukvić et al, 2022) and in accordance with the results obtained from the Schaeffler diagram (Bukvić, 2012; Bukvić et al 2022). The result from the Schaeffler diagram is shown in Figure 2.

Table 3 – Chemical compositions of the filler materials
(Bukvić, 2022; Jesenice Ironworks, 2005)
Таблица 3 – Химические составы дополнительных материалов
(Bukvić, 2022; Jesenice Ironworks, 2005)
Табела 3 – Хемијски састави додатних материјала
(Bukvić, 2022; Jesenice Ironworks, 2005)

	C	Si	Mn	Cr	Ni
MIG 18/8/6	0,08	<1.0	7	18,5	9

Table 4 – Mechanical properties of the pure weld metal filler material (Bukvić, 2022; Jesenice Ironworks, 2005)

Таблица 4 – Механические свойства присадочного материала из чистого металла сварного шва (Bukvić, 2022; Jesenice Ironworks, 2005)

Табела 4 – Механичке особине чистог метал шва додатног материјала (Bukvić, 2022; Jesenice Ironworks, 2005)

	R_e , [N/mm ²]	R_m , [N/mm ²]	A_5 , [%]	KV, [J]
MIG 18/8/6	> 380	560 do 660	35	> 40 (pri 20 °C)

The choice of a filler material is directly related to the need for the desired chemical composition. Then the composition of the filler material corresponds to the chemical composition of one of the base materials or the average chemical composition. For bonding high-alloy steel with some other less alloyed or unalloyed steel, a high-alloy filler material should be used, as shown by the position of the filler metal in Figure 2 of the Schaeffler diagram (Bukvić et al, 2022).

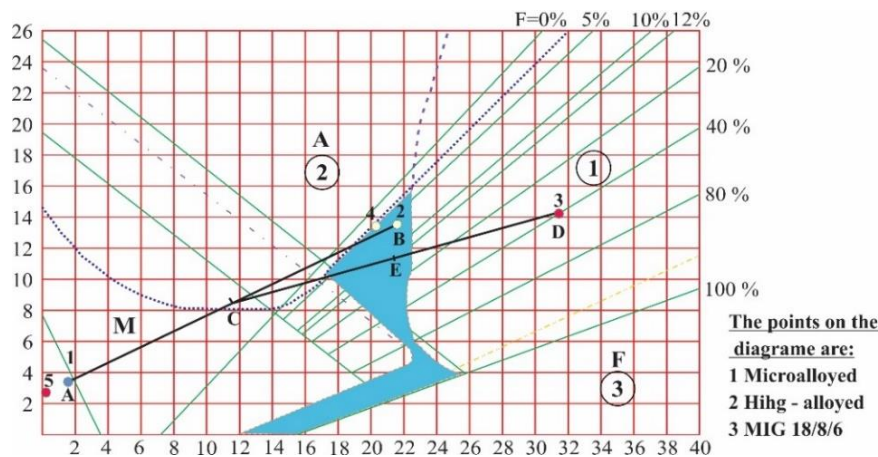


Figure 2 – Positions of base and filler materials in the Schaeffler diagram

Рис. 2 – Положение основных и дополнительных материалов на диаграмме Шеффлера

Слика 2 – Положај основних и додатних материјала у Шефлеровом дијаграму

Welding technology

The plates of the base materials are welded by the electric arc semi-automatic MIG/MAG process. A MIG/MAG welding device KEMPACT 3000+ FastMig 400 was used for welding. Two different heat inputs were applied, as shown in Tables 5 and 6. Two welded experimental plates were formed: with a maximum heat input of 8.88 [kJ/cm], plate number 1, and with a minimum heat input of 6.87 [kJ/cm], plate number 2 (Bukvić, 2012; Bukvić et al 2022).

Table 5 – Average amount of heat input during the welding of plate number 1 (Bukvić, 2012)

Таблица 5 – Среднее количество подводимого тепла при сварке пластины № 1 (Bukvić, 2012)

Табела 5 – Просечан унос количине топлоте при заваривању плоче број 1 (Bukvić, 2012)

Plate and wire designation	Welding		Average strength electricity [A]	Average voltage [V]	Average amount of heat input [kJ/cm]
	Mean time [min.]	Medium speed [cm/min]			
Plate number 1	2.22	24.2	214	26.37	8.88

Table 6 – Average input of heat during the welding of plate number 2 (Bukvić, 2012)

Таблица 6 – Среднее количество подводимого тепла при сварке пластины № 2 (Bukvić, 2012)

Табела 6 – Просечан унос количине топлоте при заваривању плоче број 2 (Bukvić, 2012)

Plate and wire designation	Welding		Average strength electricity [A]	Average voltage [V]	Average amount of heat input [kJ/cm]
	Mean time [min.]	Medium speed [cm/min]			
Plate number 2	2.19	34.15	243	30.47	6.87

The shielding gas flow was 12 l/min. A mixture of Ar and 2% O₂ gases was used as a protective atmosphere during welding (Smiljanić, 2006; Messer Tehnogas, 2008).

The welding was performed using the multi-pass advance welding technique. For each welded plate, the number of passes during welding was six and it was determined by the speed of welding, different voltage and strength of current, i.e. different amount of heat input during welding. Each plate of the base material was preheated, and the intermediate temperature was maintained by heating with a flame from a mixture of oxygen and acetylene. With each welded plate, the root passage is first welded from the inside of the groove. After that, the filling passages were welded. The

resulting welded plates were cooled in still air (Bukvić, 2012; Bukvić et al, 2022).

The welded joints were visually inspected and subjected to radiographic ventilation with γ -rays. No defects such as cracks, lack of penetration, sticking, etc. were detected.

The welded plates were machined to the same thickness of 12 mm (Bukvić, 2012; Bukvić et al, 2022).

From the obtained welded plates number 1 and 2 of the ferritic-austenitic welded joint, test specimens were cut in accordance with the standards for testing impact toughness and for determining fracture toughness at flat deformation K_{Ic} .

Test of impact toughness on an instrumented Charpy pendulum

The test of impact force on notched test specimens can provide an explanation about the behavior of a material around the crack tip, starting from the assumption that the test specimen material is sufficiently homogeneous under a plane state of stress (Miletić et al, 2020; Paris & Erdogan, 1963). Determining the energy required for fracture under established test conditions is most often used for regular control of the quality and homogeneity of a material, as well as for its processing quality control. With this test procedure, the tendency to increase brittleness during exploitation (aging) can be determined. The impact tests of the test specimens were performed in accordance with ASTM E23-95 Standard (Miletić et al, 2020; Paris & Erdogan, 1963), on the test specimens of the dimensions and appearance as in Figure 3 and in order to determine the total impact energy (Miletić et al, 2020; Paris & Erdogan, 1963).

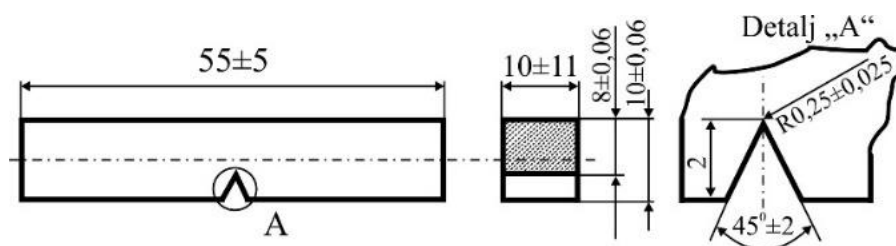


Figure 3 – Standard impact test specimen

Рис. 3 – Стандартный образец для испытания на удар

Слика 3 – Стандардна епрувета за испитивање ударне живавости

The notch position in relation to the welded joint is defined by ISO 9016:2022 Standard (ISO, 2022). The notch is made by milling so that the state of the material does not change during processing.

In bending impact load testing, fracture energy is determined as an integral quantity. The fracture energy determined in this way does not give the possibility of separating the resistance of the material related to the formation, i.e. the propagation of the crack. The impact force and time were continuously recorded during the test on an instrumented pendulum. This is how the force-time diagram was obtained. From it, it is possible to calculate the total energy E_{uk} , required for the fracture of a specimen using the formula (Miletić et al, 2020; Paris & Erdogan, 1963):

$$E_{uk} = \int_0^{t_1} F(t) \cdot v(t) \cdot dt \quad (1)$$

where: $F(t)$ – force; $v(t)$ – change in the speed of the pendulum during the break; and t – duration of fracture.

In order to evaluate the behavior of the material under impact load, it is necessary to know which part of the energy is used for the formation of the crack, and which part for the propagation of the crack. The procedure for determining the energy of crack growth through the "fatigue crack" was used. The part of the energy required to form an E_{inic} crack is calculated by the formula (Miletić et al, 2020; Paris & Erdogan, 1963):

$$E_{inic} = E_{uk} - E_{lom} \quad (2)$$

The energy of formation and the energy of crack growth are determined by this method on one specimen (unlike other procedures), which gives higher accuracy (Miletić et al, 2020; Paris & Erdogan, 1963).

Impact toughness test results on an instrumented Charpy pendulum

The impact energy was determined on an instrumented Charpy pendulum with an oscilloscope whose impact load range is 150/300 J. Standard Charpy V-notch test specimens were used during the test, as in Figure 3, and the energies were calculated by formulas (1) and (2).

Results of testing the toughness of the base material

At the very beginning, before welding, from the plate of microalloyed steel NIOMOL 490K, the test specimens were cut normal to the direction of rolling of the plate and marked with a U mark with a notch normal to the rolling direction. After that, test specimens were cut from the same plates

in the rolling direction and marked with a P, with a notch parallel to the rolling direction. The cut test specimens were tested for impact toughness. The test was performed at room temperature. The obtained results are shown in Table 7 and Figure 4.

Table 7 – Fracture energy of the test specimens made of a microalloyed steel base material

Таблица 7 – Энергия разрушения испытываемых образцов, изготовленных из микролегированной стали

Табела 7 – Енергија лома епрувета из основног материјала микролегираног челика

Material	Test specimen label	Notch place	Impact energy, E_u [J]		Crack formation energy, E_{inc} [J]		Propagation energy, E_{prop} [J]	
			By test specimen	Average value	By test specimen	Average value	By test specimen	Average value
Microalloyed steel NiOMOL 490 K	P-1	Transverse to the rolling direction	279.2	265.9	73.7	78.1	205.5	201.1
	P-2		252.6		82.5		196.7	
	U-1	Normal to the rolling direction	253.4	252.1	78.2	77.1	175.2	175
	U-2		250.8		76.1		174.7	

As it can be seen from Table 7 and from the diagram in Figure 4, the total impact energies of microalloyed steel do not differ significantly depending on where the notch is placed in relation to the plate rolling direction. The total energy is slightly higher when the notch is transverse to the rolling direction and ranges from 252.6 J to 279.2 J. When the notch is placed normally to the rolling direction, the total energy is slightly lower and has a value of 250.8 J to 253.4 J.

Table 7 and the diagrams in Figure 4 show that the energy of crack formation does not depend significantly on the position of the notch. It ranges from 78.1 J when the notch is transverse to the rolling direction to 77.1 J when the notch is normal to the rolling direction. It is observed that the crack propagation energy depends on the position of the notch. It ranges from 201.1 J when the notch is transverse to the rolling direction to 175 J when the notch is normal to the rolling direction.

The properties of high-alloy austenitic steel were not investigated, because it is known from the literature (Sedmak A. et al, 2022) that austenitic steels have good toughness at low temperatures. On pressure vessels (Golubović et al, 2018), structural changes in the base material and the HAZ were neither expected nor revealed by the examination.

energy is from 190.5 J to 218.1 J, while it is from 189.5 J to 216.3 J in the test specimen from plate 2.

Table 9 – Fracture energy of the notched test specimens in the HAZ towards the microalloyed steel

Таблица 9 – Энергия разрушения испытуемых образцов с надрезами в ЗТВ по отношению к микролегированной стали

Табела 9 – Енергија лома епрувета са зарезом у ЗУТ ка микролегираном челику

Plate no.	Test specimen label	Impact energy, E_u [J]		Formation energy, E_{inic} [J]		Propagation energy, E_{lom} [J]	
		By test specimen	Average value	By test specimen	By test specimen	Average value	By test specimen
1	1.3	218.1	204.3	68.5	63.5	149.3	140.8
	1.4	190.5		58.2		132.3	
2	2.3	189.5	202.9	61.1	67.8	128.4	135.1
	2.4	216.3		74.6		141.7	

Diagrams $F-\tau$ and $E_u-\tau$
The specimen 1.3 The specimen 2.3

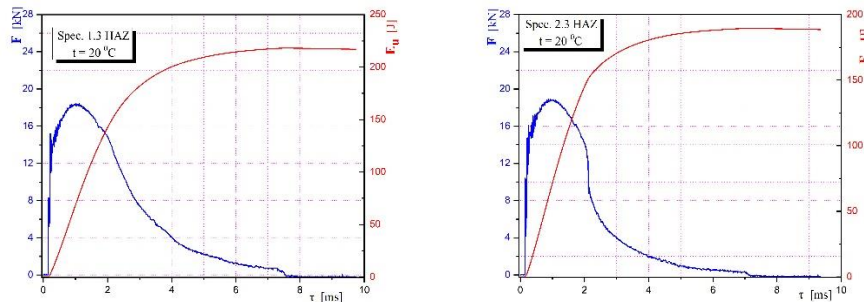


Figure 6 – Diagrams of the impact tests of the test specimens with a notch in the HAZ

Рис. 6 – Диаграммы ударных испытаний образцов с надрезом в ЗТВ
Слика 6 – Дијаграми ударних испитивања епрувета са зарезом у ЗУТ

The crack formation energy is of very uniform values. The test specimens from plate 2 have a higher crack formation energy of 67.8 J while the test specimens from plate 1 have a slightly lower crack formation energy of 63.5 J.

Crack propagation energy does not differ from plate to plate. The test specimens from experimental plate 1 have a higher crack propagation energy of 140.8 J and the test specimens from experimental plate 2 have a slightly lower crack propagation energy of 135.1 J.

Determining the fracture toughness during flat deformation K_{Ic}

Examining test specimens with a crack shows the local behavior of the material around the crack tip, starting from the assumption that the material around the crack is sufficiently homogeneous, which means that the results of the local behavior can be treated globally, i.e. they can be directly transferred to an appropriate construction. The influence of the heterogeneity of a structure and the mechanical properties of a welded joint is primarily reflected in the position of the fatigue crack tip and the characteristics of the area through which the fracture propagates (Bukvić, 2012; Zerbst et al, 2015; Kumar et al, 2016).

The test of fracture toughness during flat deformation K_{Ic} was carried out in order to determine the critical stress intensity factor K_{Ic} , i.e. the evaluation of the behavior of the components of the welded joint, weld metal and the HAZ in the presence of a crack-type defect as the most dangerous of all defects in structural materials, especially welded joints (Bukvić, 2012; Zerbst et al, 2015; Kumar et al, 2016). The test was performed at room temperature.

Two groups of test specimens were tested depending on the location of the fatigue crack tip, namely:

- Group I - test specimens with the fatigue crack tip in the filler metal,
- Group II - test specimens with the fatigue crack tip in the HAZ towards microalloyed steel.

Three-point bending test specimens (SEB) were used to determine K_{Ic} , the geometry of which is defined by ASTM E399 Standard and given in Figure 7.

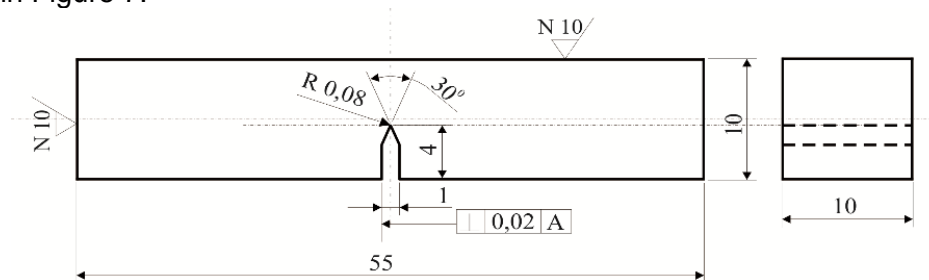


Figure 7 – Specimen for fracture mechanics testing
 Рис. 7 – Образец для испытаний на механику разрушения
 Слика 7 – Епрувета за испитивање механике лома

As defined by ASTM E399 Standard, i.e. BS 7448 Part 1, the first step was to prepare a test specimen, i.e. to form a fatigue crack. The fatigue crack on the fractured test specimen marked 1.5 under c is shown in Figure 8. Approximately 50% of the final length of the fatigue crack was produced at the maximum fatigue force $F_{max} = 0.4 \cdot F_L$. In this case, the minimum force was $F_{min} = 0.1 \cdot F_{max}$. The fatigue crack was formed on an AMSLER high-frequency pulsator⁴. The condition of flat state of deformation is not satisfied according to ASTM E399:

$$B \geq 2.5 \cdot \left(\frac{K_{Ic}}{R_{p0.2}} \right)^2 \quad (3)$$

In that case, instead of applying linear-elastic fracture mechanics (LEML) defined by ASTM E399 Standard, elasto-plastic fracture mechanics (EPML) defined by ASTM E813, ASTM E1152, ASTM E1820-18 and BS 7448 Part 1 and 2 Standards was applied. The purpose of using elasto-plastic fracture mechanics is to determine the value of the critical stress intensity factor K_{Ic} indirectly via the critical J-integral J_{Ic} , i.e. to monitor the crack growth under the conditions of pronounced plasticity. The behavior of the elasto-plastic material, which also includes the components of the welded joint, during a stable crack growth can be described by the $J-\Delta a$ diagram, where Δa is crack growth (Bukvić, 2012; Zerbst et al, 2015; Kumar et al, 2016).

Based on the obtained data, a $J-\Delta a$ curve is constructed, on which a regression line is constructed according to ASTM E1152. The critical J-integral J_{Ic} is obtained from the obtained regression line. Knowing the values of the critical J_{Ic} integral, one can calculate the value of the critical stress intensity factor or the fracture toughness at flat deformation K_{Ic} , using dependence (4) ASTM E399:

$$K_{Ic} = \sqrt{\frac{J_{Ic} \cdot E}{1 - \nu^2}} \quad (4)$$

where: E – modulus of elasticity and ν – Poisson's ratio.

The critical value of the stress intensity factor K_{Ic} was determined using the method of one test specimen with successive loading and unloading (Bukvić, 2012; Zerbst et al, 2015; Kumar et al, 2016).

Based on the data collected from a tensile machine (force transducer and COD transducer), the diagrams of force F –Crack Mouth Opening Displacement δ (CMOD–Crack Mouth Opening Displacement) were constructed.

These diagrams are the basis for determining the critical value of the J-integral J_{Ic} . However, in order to determine the length of the crack Δa , it is necessary to measure the length of the original fatigue crack a_z (Bukvić, 2012; Zerbst et al, 2015; Kumar et al, 2016).

Determination of K_{Ic} in the test specimens with a notch in the filler metal

The results of measuring the length of the fatigue crack are given in Table 10 while the diagrams F – δ and J – Δa for the test specimens with a notch in the filler metal are given in Figures 8 and 9.

Table 10 – Fatigue crack lengths of the specimens with a notch in the filler metal

Таблица 10 – Длина усталостной трещины образца с надрезом в металле шва

Табела 10 – Дужине заморне прслине епрувета са зарезом у метал шаву

Plate no.	Test specimen label	Fatigue crack length, a_z [mm]					Average value, a_{zSR} [mm]
		a_{z1}	a_{z2}	a_{z3}	a_{z4}	a_{z5}	
1	1.5	2.85	2.93	3.34	3.67	3.26	3.21
2	2.5	2.42	2.90	2.65	2.92	2.92	2.762

The calculated values of the critical stress intensity factor, K_{Ic} , are given in Table 11 for the test specimens with a notch in the filler metal. In the calculation for fracture toughness at flat deformation K_{Ic} , a single value for the modulus of elasticity at room temperature of 210 GPa was used.

The fracture toughness values K_{Ic} of the specimens with a notch in the filler metal range from 125.1 MPa $m^{1/2}$ to 130.5 MPa $m^{1/2}$. The values do not differ significantly, because it is the same filler material, regardless of the difference in the amount of heat input during welding.

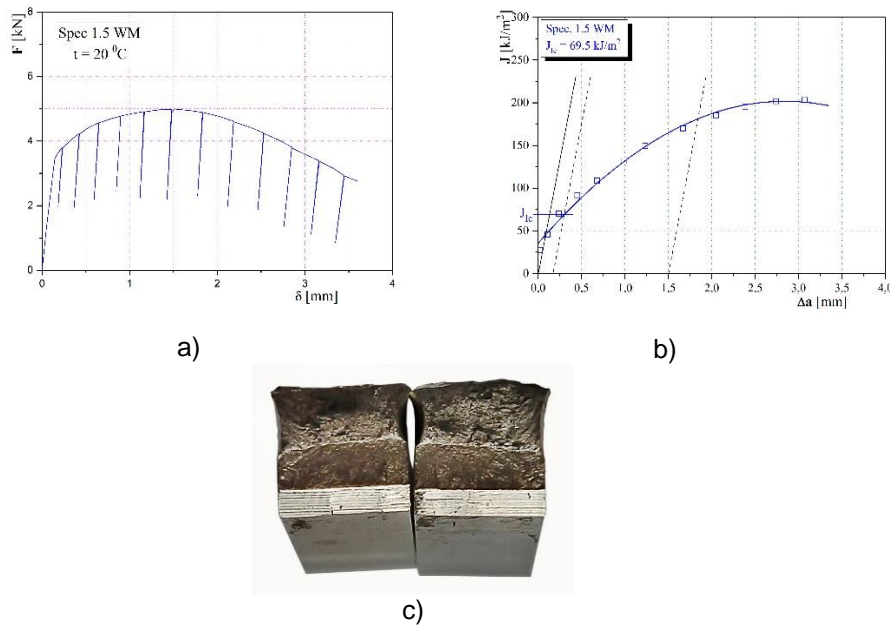


Figure 8 – (a) F – δ diagram, (b) J – Δa diagram and (c) a broken test specimen 1.5 with a notch in the filler metal

Рис. 8 – Диаграммы F – δ (а), J – Δa (b) и (с) разрушенный образец 1,5 с надрезом в металле шва

Слика 8 – (а) дијаграми F – δ , (b) J – Δa и (с) преломљена епрувета 1,5 са зарезом у метал шаву

Table 11 – K_{Ic} values of the specimens with a notch in the filler metal

Таблица 11 – Значения образцов K_{Ic} с надрезом в металле шва

Табела 11 – Вредности K_{Ic} епрувета са зарезом у метал шаву

Plate no.	Test specimen label	Critical J–integral, J_{Ic} [kJ/m ²]	Critical stress intensity factor, K_{Ic} [MPa m ^{1/2}]	Critical crack length, a_c [mm]
1	1.5	69.5	125.1	93.4
2	2.5	75.6	130.5	100.9

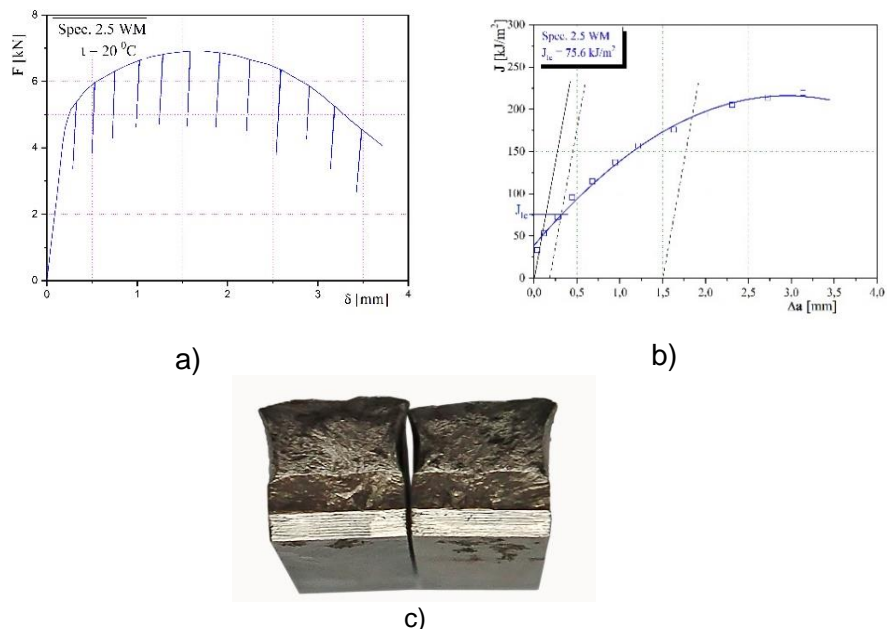


Figure 9 – (a) $F-\delta$ diagram, (b) $J-\Delta a$ diagram and (c) a broken test specimen 2.5 with a notch in the filler metal

Рис. 9 – Диаграммы $F-\delta$ (а), $F-\delta$ (b) и (с) в разрушенных образцах 2.5 с надрезом в металле шва

Слика 9 – (а) дијаграми $F-\delta$, (b) $F-\delta$ и (с) преломљена епрувета 2,5 са зарезом у метал шаву

Determination of K_{Ic} in the test specimens with a notch in the HAZ

The results of measuring the fatigue crack length in the test specimens with a notch in the HAZ towards microalloyed steel are given in Table 12 and in the $F-\delta$ and $J-\Delta a$ diagrams in Figures 10 and 11.

Table 12 – Fatigue crack lengths of the notched test specimens in the HAZ at room temperature

Таблица 12 – Длины усталостных трещин на испытуемых образцах с надрезами в ЗТВ при комнатной температуре

Табела 12 – Дужине заморне прслине епрувета са зарезом у ЗУТ на собној температури

Plate no.	Test specimen label	Fatigue crack length, a_z [mm]					Average value, a_{zSR} [mm]
		a_{z1}	a_{z2}	a_{z3}	a_{z4}	a_{z5}	
1	1.6	3.46	3.47	3.28	2.41	2.34	2.99
2	2.6	2.17	3.56	3.19	3.43	3.31	3.13

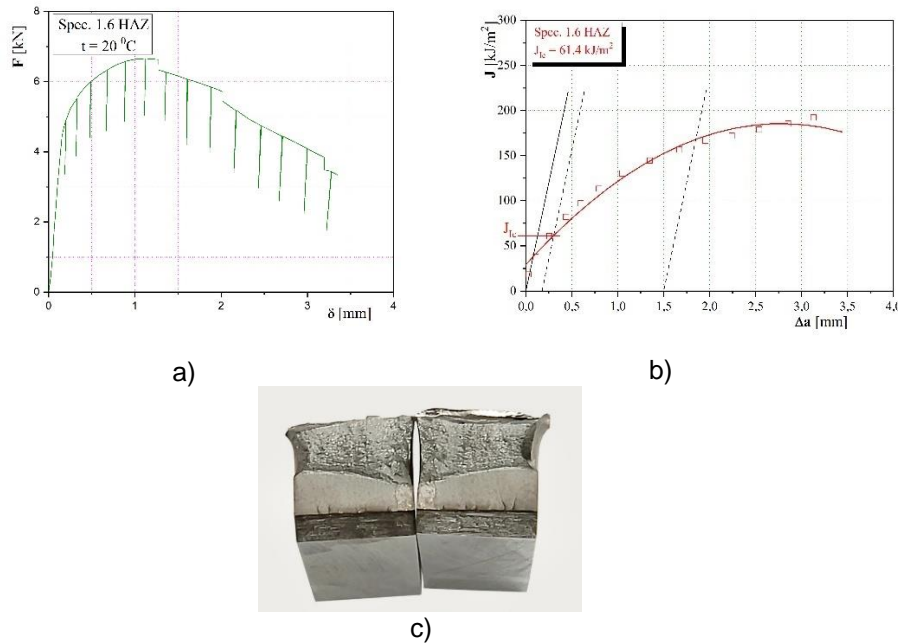


Figure 10 – (a) $F - \delta$ diagram, (b) $J - \Delta a$ diagram and (c) a broken test specimen 1.6 with a notch in the HAZ towards the microalloyed base material

Рис. 10 – (а) диаграмма $F - \delta$, (b) $J - \Delta a$ и (с) разрушенный испытуемый образец 1.6 с надрезом в ЗТВ со стороны микролегированного основного материала

Слика 10 – (а) дијаграми $F - \delta$, (б) $J - \Delta a$ и (с) преломљена епрувета 1,6 са зарезом у ЗУТ са стране микролегираног основног материјала

Table 13 – Fatigue crack lengths of the notched test specimens in the HAZ

Таблица 13 – Длине усталостних трещина на испитуемим образцима с надрезима в ЗТВ

Табела 13 – Дужине заморне прслине епрувета са зарезом у ЗУТ

Plate no.	Test specimen label	Critical J-integral, J_{Ic} [kJ/m ²]	Critical stress intensity factor, K_{Ic} [MPa m ^{1/2}]	Critical crack length, a_c [mm]
1	1.6	61.4	117.6	82.5
2	2.6	69.5	125.1	92.7

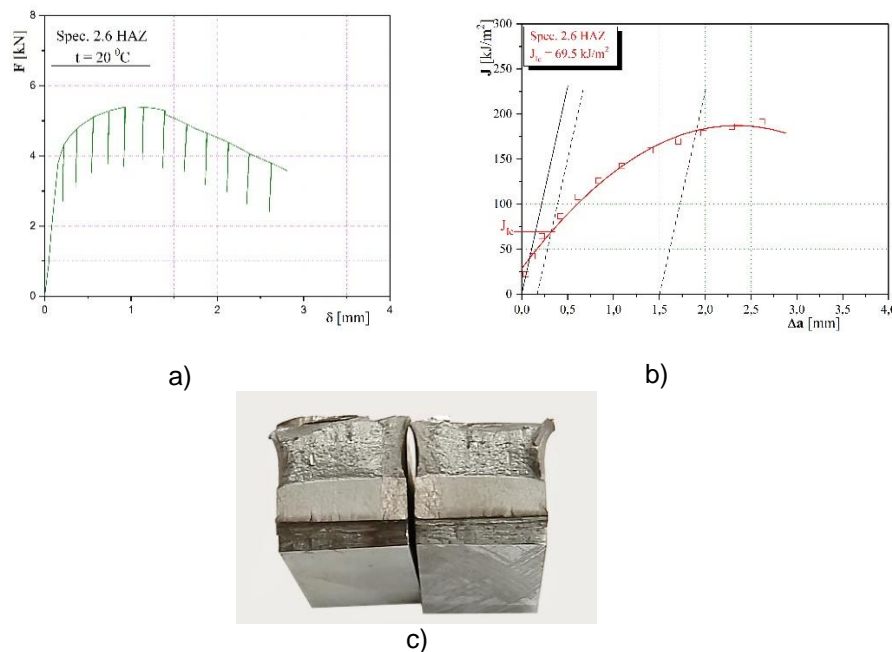


Figure 11 – (a) $F - \delta$ diagram, (b) $J - \Delta a$ diagram and (c) a broken test specimen 2.6 with a notch in the HAZ towards the microalloyed base material
 Рис. 11 – (а) диаграмма $F - \delta$, (b) $J - \Delta a$ и (с) разрушенный испытуемый образец 2.6 с надрезом в ЗТВ со стороны микролегированного основного материала
 Слика 11 – (а) дијаграма $F - \delta$, (б) $J - \Delta a$ и (с) преломљена епрувета 2,6 са зарезом у ЗУТ са стране микролегираног челика

The obtained values of fracture toughness K_{Ic} of the test specimens with a notch in the HAZ towards microalloyed steel, shown in Table 13, range from 117.6 $\text{MPa m}^{1/2}$ to 125.1 $\text{MPa m}^{1/2}$. The values do not differ significantly, which means that a different amount of heat input during welding had no effect.

Analysis of the results

In practice, different base and filler materials are used for welding in order to optimise constructions. The economy of construction is not the only reason for such use of materials. For example, storage tanks for liquid petroleum products are made of different materials. This paper deals with base materials with different chemical compositions and filler materials that have similar characteristics to one of base materials, i.e. to austenitic high-alloy steel. In such cases, different microstructures can be expected

to appear in welded joints. All this makes it difficult to predict the behaviour of such joints in use.

Welding with the filler material MIG 18/8/6 yielded two welded experimental plates, marked 1 and 2, where different amounts of heat input were used.

Experimental plates 1 and 2 were welded with the highest and lowest allowed amount of heat input. It is noted that the difference in heat input is about 30%. The obtained values of the quantity of input heat represent, in this case, the limit values for the chosen welding procedure and the filler material.

According to the Schaeffler diagram (Figure 2), it is possible to use the filler material MIG 18/8/6 during welding because the result of this bonding is in the safe area.

In testing microalloyed steel toughness at room temperature, it was observed that high values of total energy were obtained regardless of the direction in which either the test specimens or the notches were cut (transverse or normal to the rolling direction). The total impact energy is 5.3% lower for the test specimens cut transversely to the rolling direction and with their notch normal to the rolling direction. From the obtained results, the energies of crack propagation are higher than the energies of formation, which indicates the fact that the examined material is ductile.

The total impact energy obtained by testing the test specimens with a notch in the metal seam from experimental plates 1 and 2 shows that the highest achieved total energy is for the test specimens from plate 2, and a total energy lower by 3% was obtained for the test specimens from plate 1. In the tested cases, the ductile component is greater than the brittle one, so it can be concluded that experimental plates 1 and 2 with a notch in the metal seam behaved as ductile at room temperature.

The comparison of the obtained impact toughness values for the test specimens with a notch in the HAZ towards microalloyed steel from plates 1 and 2 shows that the values are high and slightly lower than the toughness values in the microalloyed steel test specimens. This decrease in toughness is due to the growth of grains in the HAZ and the appearance of bainite in the structure. In all tested samples, the energy of propagation is higher than the energy of formation. This leads to the conclusion that the test specimens were ductile at room temperature.

Observing the obtained values of the critical stress intensity factor K_{Ic} for the test specimens with a notch in the metal seam, one can notice that different amounts of heat input during welding did not give significant differences in the values of K_{Ic} .

The obtained critical crack lengths are adequate to the obtained K_{Ic} values, so the highest value is for plate 2, and a slightly smaller one for plate 1. It can be concluded, based on the values of the critical crack lengths and fatigue crack lengths for the test specimens with a notch in the metal seam, that the best characteristics in the presence of a crack-type defect will be shown by plate 2 followed closely by plate 1.

Observing the obtained values of the critical stress intensity factor K_{Ic} for the test specimens with a notch in the HAZ towards microalloyed steel leads to the conclusion that plate 2 has the highest values while plate 1 has a lower value by 6%.

The obtained critical crack lengths are adequate to the obtained K_{Ic} values, so the highest value is obtained by plate 2 while plate 1 has a lower value by 11%.

Conclusions

Based on the test results, the following conclusions can be drawn:

1. The resistance of microalloyed steel to crack formation and growth is uniform regardless of whether test specimens are cut in the rolling direction of the experimental plates or cut normal to the rolling direction of the plates;
2. The obtained impact energies from the test specimens with a notch in the metal seam are lower than the impact energies from the test specimens with a notch in the HAZ by about 35%;
3. Different amount of heat input during welding with the same filler material does not give a difference in the obtained impact energy;
4. A higher value of the critical stress intensity factor K_{Ic} was obtained for the test specimens with a notch in the metal seam compared to the test specimens with a notch in the HAZ;
5. The critical length of the cracks is smaller in the test specimens with a notch in the HAZ by about 10%; and
6. If a construction made of the materials used in this study is exposed to a stress lower than the yield stress and if there is a crack in their welded joint smaller than the critical one, there is no risk of fracture.

References

-ASTM International. 1989. *ASTM E813 (1989) Standard Test Method for J_{Ic} a Measure of Fracture Toughness*. West Conshohocken, PA, USA: ASTM International.

-ASTM International. 2017. *ASTM E399-90 (1997) Standard Test Method for Plane-Strain Fracture Toughness of Metallic Materials*. Available at: <https://doi.org/10.1520/E0399-90R97>.

-ASTM International. 2019. *ASTM E1820-18 Standard Test Method for Measurement of Fracture Toughness*. Available at: <https://doi.org/10.1520/E1820-18>.

-ASTM International. 2021. *ASTM E1152-95 Test Method for Determining J-R Curves (Withdrawn 1997)* [online]. Available at: <https://www.astm.org/standards/e1152> [Accessed: 20 January 2023].

-British Standards Institution (BSI). 2023. *Multi-part Document BS 7448-Fracture mechanics toughness tests*. London, UK: The British Standards Institution (BSI). Available at: <https://doi.org/10.3403/BS7448>.

Bukvić, A. 2012. *Research of the influence of additional materials on the behavior of ferritic austenitic welded joints*. Ph.D. thesis. Belgrade: University of Belgrade - Faculty of Mechanical Engineering (in Serbian).

Bukvić, A., Petrović, D., Radisavljević, I. & Dimitrić, S. 2022. Influence of heat input on the tensile properties of austenitic-ferritic welded joints. *Vojnotehnički glasnik/Military Technical Courier*, 70(2), pp.409-432. Available at: <https://doi.org/10.5937/vojtehg70-36252>.

Golubović, T., Sedmak, A., Spasojević-Brkić, V., Kirin, S. & Veg, E. 2018. Welded joints as critical regions in pressure vessels - case study of vinyl-chloride monomer storage tank. *Hemijska industrija*, 72(4), pp.177-182. Available at: <https://doi.org/10.2298/HEMIND171009006G>.

-ISO. 2022. *ISO 9016:2022 Destructive tests on welds in metallic materials - Impact tests - Test specimen location, notch orientation and examination* [online]. Available at: <https://www.iso.org/standard/81122.html> [Accessed: 20 January 2023].

-Jesenice Ironworks. 2022. *Additional welding materials, catalog*. Jesenice Ironworks.

Jovičić, R. 2007. *Analysis of the effect of cracks on the integrity of ferritic-austenitic welded joints*. Ph.D. thesis. Belgrade: University of Belgrade - Faculty of Mechanical Engineering (in Serbian).

Kumar, Y., Venugopal, S., Sasikala, G., Albert, S.K. & Bhaduri, A.K. 2016. Study of creep crack growth in a modified 9Cr–1Mo steel weld metal and heat affected zone. *Materials Science and Engineering: A*, 655, pp.300-309. Available at: <https://doi.org/10.1016/j.msea.2015.12.053>.

-Messer Tehnogas. 2008. *Technical documentation: Shielding gases in welding*. Belgrade, Serbia: Messer Tehnogas AD (in Serbian).

Miletić, I., Ilić, A., Nikolić, R.R., Ulewicz, R. Ivanović, L. & Sczygiol, N. 2020. Analysis of Selected Properties of Welded Joints of the HSLA Steels. *Materials*, 13(6), art.ID:1301. Available at: <https://doi.org/10.3390/ma13061301>.

Paris, P. & Erdogan, F. 1963. A Critical Analysis of Cracks Propagation Laws. *Journal of Basic Engineering*, 85(4), pp.528-533. Available at: <https://doi.org/10.1115/1.3656900>.

Rabbolini, S., Beretta, S., Foletti, S. & Riva, A. 2015. Short crack propagation in LCF regime at room and high temperature in Q & T rotor steels. *International Journal of Fatigue*, 75, pp.10-18. Available at: <https://doi.org/10.1016/j.ijfatigue.2015.01.009>.

Sedmak, A., Arsić, M., Milovanović, N., Opačić, M. & Đorđević, B. 2022. Structural Integrity Analysis of a Kaplan Turbine Cover. *Procedia Structural Integrity*, 37, pp.263-268. Available at: <https://doi.org/10.1016/j.prostr.2022.01.083>.

Smiljanić, M. 2006. Zaštitni gasovi u zavarivanju. In: *DUZS Seminar*, pp.36-43, July 2006. (in Serbian).

Zerbst, U., Klingner, C. & Clegg, R 2015. Fracture mechanics as a tool in failure analysis - Prospects and limitations. *Engineering Failure Analysis*, 55, pp.376-410. Available at: <https://doi.org/10.1016/j.engfailanal.2015.07.001>

Анализ ударной вязкости и критического коэффициента интенсивности напряжений K_{Ic} в ферритно-аустенитных сварных соединениях с различным подводом тепла

Александар Г. Буквич^а, **корресподент**, Далибор П. Петровић^а, Игор З. Радисавлевић^б, Саша С. Димитрић^а

^а Университет обороны в г. Белград, Военная академия, г. Белград, Республика Сербия

^б Министерство обороны Республики Сербия, Военно-технический институт, г. Белград, Республика Сербия

РУБРИКА ГРНТИ: 81.35.39 Сварные металлоконструкции,
81.35.13 Технология и оборудование сварочного производства

ВИД СТАТЬИ: оригинальная научная статья

Резюме:

Введение/цель: В любой конструкции всегда имеется несколько критических точек, которые могут оказаться источниками образования дефектов. Все эти критические места однозначно должны приниматься во внимание при оценке безопасности, которая нацелена на выявление наиболее неблагоприятных факторов эксплуатации и оценку локальной безопасности соединений. Сегодня в металлоконструкциях все чаще встречаются соединения различного состава. В связи с требованиями энергоэффективности и экологии при строительстве электростанций, химических объектов и пр. сварные соединения микролегированных ферритных сталей с высоколегированными аустенитными сталями встречаются все чаще. Испытания таких сварных соединений проводились на резервуарах для нефтепродуктов, части корпуса которого изготовлены из микролегированной ферритной стали, а конструкция крыши – из высоколегированной аустенитной стали.

Методы: В данной статье представлены результаты экспериментального анализа распространения трещины в аустенитно-ферритном сварном соединении. Сварка выполнялась методом MIG с двумя различными тепловыми подводами, причем

использовался один и тот же присадочный материал MIG 18/8/6. Были испытаны два типа сварных пластин. В статье описаны характеристики основных, дополнительных и расходных материалов, а также технологии сварки. Для определения ударных свойств и параметров механики разрушения были изготовлены испытательные образцы с надрезами и начавшимся разрушением по типу трещины.

Результаты: Целью данного исследования являлось сравнение полученных результатов ударной вязкости, вязкости разрушения и деформации в плоскости феррито-аустенитного сварных соединений. Также в статье приведена оценка результатов, полученных при испытании экспериментальных пластин, свариваемых с различным количеством подводимого тепла.

Выводы: По результатам испытаний выявлена зависимость геометрии расширения трещины от условий напряжения. Таким образом можно определить значения параметров, описывающих поведение материала, как при линейно-упругой, так и при упруго-пластической механике разрушения.

Ключевые слова: ферритно-аустенитное сварное соединение, ударная вязкость, критический коэффициент интенсивности напряжений K_{Ic} .

Анализа ударне живавости и критичног фактора интензитета напона K_{Ic} код феритно-аустенитних заварених спојева различитим уносом топлоте

Александар Г. Буквић^а, аутор за преписку, Далибор П. Петровић^а, Игор З. Радисављевић^б, Саша С. Димитрић^а

^а Универзитет одбране у Београду, Војна академија, Београд, Република Србија

^б Министарство одбране Републике Србије, Војнотехнички институт, Београд, Република Србија

ОБЛАСТ: машинство, машински материјали
ВРСТА ЧЛАНКА: оригинални научни рад

Сажетак:

Увод/циљ: Критична места конструкција извор су могућих дефеката, па се морају узети у обзир при процени сигурности, где ће се сагледати најнеповољнији експлоатациони фактори и проценити локална сигурност споја. Данас је све учесталија примена разнородних спојева у металним конструкцијама. Због економичности и екологије, при изградњи енергетских, хемијских или неких других постројења све чешће се срећу заварени спојеви микрولةгираних феритних челика са високолегираним аустенитним челицима. Одговарајућа испитивања вршена су на

резервоарима за нафтне деривате, који се израђују од делова оплате од микролегираног феритног челика и кровне конструкције од високолегираног аустенитног челика.

Метод: У раду је извршена експериментална анализа ширења прслине код феритно-аустенитног завареног споја. Заваривање је изведено МИГ поступком заваривања са два различита уноса количине топлоте, а коришћен је исти додатни материјал МИГ 18/8/6. Испитиване су две врсте заварених плоча. Наведене су карактеристике основних, додатних и помоћних материјала и технологија заваривања. Израђене су епрувете са зарезом са иницираном грешком типа прслине ради одређивања ударних својстава и параметара механике лома.

Резултати: Спроведена истраживања имала су за циљ да упореде добијене резултате ударне жилавости и жилавости лома при равној деформацији код феритно-аустенитног завареног споја. Дата је и оцена добијених резултата при испитивању експерименталних плоча које су заварене различитим уносом количине топлоте.

Закључак: Резултати испитивања јесу успостављање зависности геометрије покретне прслине и услова напрезања за даље ширење прслине. Омогућено је одређивање износа параметара који описују понашање материјала, како у линеарно-еластичној, тако и у еластично-пластичној механици лома.

Кључне речи: феритно-аустенитни заварени спој, ударна жилавост, критични фактор интензитета напона K_{Ic} .

Paper received on / Дата получения работы / Датум пријема чланка: 23.01.2023.
Manuscript corrections submitted on / Дата получения исправленной версии работы / Датум достављања исправки рукописа: 23.03.2023.
Paper accepted for publishing on / Дата окончательного согласования работы / Датум коначног прихватања чланка за објављивање: 25.03.2023.

© 2023 The Authors. Published by Vojnotehnički glasnik / Military Technical Courier (www.vtg.mod.gov.rs, втг.мо.упр.срб). This article is an open access article distributed under the terms and conditions of the Creative Commons Attribution license (<http://creativecommons.org/licenses/by/3.0/rs/>).

© 2023 Авторы. Опубликовано в «Военно-технический вестник / Vojnotehnički glasnik / Military Technical Courier» (www.vtg.mod.gov.rs, втг.мо.упр.срб). Данная статья в открытом доступе и распространяется в соответствии с лицензией «Creative Commons» (<http://creativecommons.org/licenses/by/3.0/rs/>).

© 2023 Аутори. Објавио Војнотехнички гласник / Vojnotehnički glasnik / Military Technical Courier (www.vtg.mod.gov.rs, втг.мо.упр.срб). Ово је чланак отвореног приступа и дистрибуира се у складу са Creative Commons licencom (<http://creativecommons.org/licenses/by/3.0/rs/>)

